PERGAMON

International Journal of Heat and Mass Transfer 45 (2002) 1393–1405

International Journal of HEAT and MASS TRANSFER

www.elsevier.com/locate/ijhmt

On a subgrid-scale heat flux model for large eddy simulation of turbulent thermal flow

Shia-Hui Peng *, Lars Davidson

Department of Thermo and Fluid Dynamics, Chalmers University of Technology, 412-96 Gothenborg, Sweden

Received 13 November 2000; received in revised form 7 August 2001

Abstract

A non-linear subgrid-scale (SGS) heat flux model is introduced in large eddy simulation for turbulent thermal flows. Unlike the linear isotropic eddy diffusivity model, the proposed model accounts for the SGS heat flux in terms of the large-scale strain-rate tensor and the temperature gradients. This is equivalent to using a tensor diffusivity. The model is to some extent similar to a scale-similarity model subjected to a Taylor expansion for the filtering operation. The formulation leading to the present proposal is discussed. The model is examined in LES for a buoyant flow in an infinite vertical channel with two differentially heated side walls. It is shown that the proposed model reproduces reasonable results as compared with the isotropic SGS diffusivity model and DNS data. © 2002 Published by Elsevier Science Ltd.

1. Introduction

The momentum of fluid motion in turbulent thermal flows is closely coupled with the thermal energy transport due to the buoyant force in the gravitational field. The buoyancy significantly characterizes the turbulence production and evolution process and consequently affects the flow structure. One of the well-known examples of thermal flows is the Rayleigh–Bénard (RB) convection, which consists of a fluid layer between two differently heated horizontal walls where the lower wall has a higher surface temperature than the upper wall. The turbulent RB convection is characterized by large-scale coherent vortical structures and unsteadiness associated with plumes, thermal and convective cells, where the turbulence is generated mainly in the wall boundary layer and carried away by the large-scale structure. Such a large-structure dominant flow feature has indeed rendered large eddy simulation (LES) a remarkable success.

Other typical thermal flows include those occurring in a confined cavity and in an infinite vertical channel with two differentially heated side walls. In such flows, a horizontal temperature gradient is generated that is perpendicular to the gravitational acceleration. For the buoyant flow in confined cavity at a moderately high Rayleigh number, the boundary layer along the heated/cooled vertical wall will evolve towards turbulence undergoing a transition stage. While sharing some common heat transfer features near the vertical walls, the buoyant flow arising in a vertical channel with an infinite height (hereafter termed *infinite cavity*) possesses its own dynamics of turbulence. The fully developed buoyant flow in an infinite cavity is statistically of a one-dimensional type with no thermal stratification in the direction of buoyancy. A linear isotropic eddy diffusivity Reynolds averaged Navier–Stokes equations (RANS) model will fail to reproduce the streamwise turbulent heat flux and will estimate a zero buoyant generation as the mean temperature gradient vanishes in this direction. By contrast, a number of measurements have shown that in a simple shear flow with only a cross-stream temperature gradient, the streamwise heat flux is often significantly larger than the wall-normal one.

Apart from RANS modeling, LES has gained increasing implementations for turbulent thermal flows. Various subgrid scale (SGS) models have been applied and shown encouraging performance, where the RB convection has primarily been studied, see e.g. [1–3]. For

* Corresponding author. Also at FFA, Swedish Defense Research Agency, 172 90 Stockholm, Sweden. Tel.: +46-8-5550-4325; fax: +46-8-5550-4306.

E-mail address: peng@foi.se (S.-H. Peng).

0017-9310/02/$ - see front matter
PII: S0017-9310(01)00254-X

Nomenclature

C	model coefficients with various subscripts
g_i	gravitational acceleration vector, $g_i = (-g, 0, 0)$
h	width between two vertical isothermal walls
h_i	SGS heat flux components
k	wave number
Pr	Prandtl number
Pr_t	SGS Prandtl number
Ra	Rayleigh number
t	time
$\bar{u}_i$	filtered velocity components
u'_i	resolved velocity fluctuations
x_i	Cartesian body axes
α	viscous diffusivity
α_t	SGS eddy diffusivity
β	thermal expansion coefficient
δ_{ij}	Kronecker delta
$\bar{\Delta}$	size of grid filter
ε	dissipation rate
ρ	density
Θ_r	reference temperature
$\bar{\theta}$	filtered temperature
$\mathscr{T}$	SGS timescale
τ	turbulent timescale
τ_{ij}	SGS stress tensor
ν	molecular kinematic viscosity
ν_t	SGS eddy viscosity
$\langle\rangle$	time and/or spatial averaging

Subscripts

b	buoyancy
rms	root mean square
SGS	subgrid scale

Superscript

+	normalized quantity by wall parameters

isothermal turbulent flows, on the other hand, remarkable effort has been put into modeling the SGS stress by means of a priori and a posterior tests. Among others, some non-linear SGS stress models have been proposed and tested by Lund and Novikov [4]. More recently, Kosovic [5] proposed a non-linear SGS stress model based on the constitutive theory. This model is able to considerably improve the prediction over the Smagorinsky model when applied to a neutral shear-driven atmospheric boundary layer. In spite of these and other developments in modeling the SGS stress, the modeling of the SGS heat flux in LES for turbulent thermal flows has often been based on the isotropic eddy diffusivity model through a linear alignment with the large-scale temperature gradient. The present work introduces a non-linear form based on a tensor diffusivity for the SGS heat flux modeling, which is somewhat analogous to the RANS modeling, where the heat flux is expressed in terms of the large-scale velocity deformation and temperature gradients in all directions. The resulting formulation turns out to be similar to the scale-similarity model undergoing a Taylor expansion for the filtering operation as proposed by Leonard [6]. The proposed SGS heat flux model is incorporated into the dynamic procedure and examined in large eddy simulation for the turbulent buoyant flow arising in an infinite cavity. The performance of the proposed model is analyzed in comparison with the isotropic eddy diffusivity model.

The model for the SGS turbulence and heat transfer is presented in Section 2. The resulting SGS heat flux model is then incorporated into the dynamic procedure to determine the model coefficient. In Section 3 the model is applied to a fully developed turbulent buoyant flow in an infinite cavity with a Rayleigh number of $Ra = 5.4 \times 10^5$. The performance of the model is analyzed on the basis of the simulation results. Some conclusions are then made in Section 4.

2. Model description

The basic philosophy of LES is to explicitly simulate the large-scale motion on which the effect of small scales is modeled. To distinguish between the large scales and small scales, a spatial filtering operation is used to decompose the flow variables. The effect of the small scales on the resolved turbulence is represented in terms of the SGS stresses and heat fluxes. Applying the filtering operation to the Navier–Stokes equations and the thermal energy equation leads to the governing equations for the large-scale momentum and thermal energy transport. For incompressible flow, this yields

$$\frac{\partial \bar{u}_i}{\partial t} + \frac{\partial}{\partial x_j}(\bar{u}_i, \bar{u}_j) = -\frac{1}{\rho}\frac{\partial \bar{p}}{\partial x_i} + \nu \frac{\partial^2 \bar{u}_i}{\partial x_j \partial x_j} - \frac{\partial \tau_{ij}}{\partial x_j} - g_i \beta(\bar{\theta} - \Theta_r) \tag{1}$$

and

$$\frac{\partial \bar{\theta}}{\partial t} + \frac{\partial}{\partial x_j}(\bar{u}_j \bar{\theta}) = \alpha \frac{\partial^2 \bar{\theta}}{\partial x_j \partial x_j} - \frac{\partial h_j}{\partial x_j}. \tag{2}$$

Note that the coordinate system in this work has been defined by taking the x (x_1) direction as the streamwise (vertical) direction and y (x_2) and z (x_3) as the wall-normal and spanwise directions, respectively.

2.1. The SGS stress model

The SGS stress appearing in the filtered Navier–Stokes equations is responsible for the energy transfer between the large-scale and the SGS eddies. This means that it should provide adequate dissipation, which is actually the flux of turbulent kinetic energy transferred through the inertial subrange. Since the dissipation rate is essentially determined by the large-scale motion, it is plausible to model the SGS stresses in terms of some large-scale properties. Indeed, the SGS stress tensor has often been modeled in alignment with the large-scale strain-rate tensor, $\bar{S}_{ij}$, through the SGS eddy viscosity, ν_t, i.e.,

$$\tau_{ij} = \overline{u_i u_j} - \bar{u}_i \bar{u}_j = -2\nu_t \bar{S}_{ij} + \frac{\delta_{ij}}{3}\tau_{kk} \tag{3}$$

with

$$\bar{S}_{ij} = \frac{1}{2}\left(\frac{\partial \bar{u}_i}{\partial x_j} + \frac{\partial \bar{u}_j}{\partial x_i}\right). \tag{4}$$

The SGS eddy viscosity has usually been cast in the relation of $\nu_t \propto L_{\mathrm{SGS}}^2 \bar{\omega}$, where L_{SGS} represents the SGS turbulent length scale and $\bar{\omega}$ is the reciprocal of SGS turbulent timescale, $\bar{\omega} = 1/\mathscr{T}_{\mathrm{SGS}}$. It is natural to relate the length scale, L_{SGS}, to the filter width, $\bar{\Delta}$, since the most active subgrid scales are those closest to the filtering cutoff. This thus suggests

$$\nu_t = C\bar{\Delta}^2\bar{\omega}. \tag{5}$$

To argue the SGS time scaling ($\bar{\omega}$ or $\mathscr{T}_{\mathrm{SGS}}$), a hypothesis has been often employed by assuming that a local equilibrium holds for small scale (i.e. subgrid scale) turbulence. Consequently, the transport of the local SGS kinetic energy is assumed in a simple balance sustained by its production and the viscous dissipation, i.e. $P_{k\mathrm{SGS}} = \varepsilon$, from which the timescale, $\mathscr{T}_{\mathrm{SGS}}$, can be derived. Applying this hypothesis to isothermal turbulent flows yields the well-known Smagorinsky model, where the SGS time scaling, $\bar{\omega}$, in (5) is set as the magnitude of the local resolved strain-rate tensor, viz:

$$\bar{\omega} = |\bar{S}| = \sqrt{2\bar{S}_{ij}\bar{S}_{ij}}. \tag{6}$$

For turbulent buoyant flows, the buoyant production may be included in the equilibrium argument for the subgrid scales. As a result, Eidson [7] proposed an SGS model in which the SGS timescale is explicitly modified by the buoyancy. This gives

$$\bar{\omega} = \left(|\bar{S}|^2 - \frac{g\beta}{Pr_t}\frac{\partial \bar{\theta}}{\partial x_j}\delta_{1j}\right)^{1/2}. \tag{7}$$

Note that the linear eddy diffusivity assumption has been used here for the SGS heat flux.

With the Eidson model, the eddy viscosity must be constrained to be equal to zero when

$$|\bar{S}|^2 < \frac{g\beta}{Pr_t}\frac{\partial \bar{\theta}}{\partial x_j}\delta_{1j}$$

to avoid incurring non-real solutions, while this situation is often encountered in thermally stratified flows. To preserve the direct influence of buoyancy in the ν_t formulation and to relax the constraint inherent in the Eidson model, a modified buoyancy model was proposed in which the SGS time scaling is weighted with the magnitude of the strain-rate tensor [3]. This gives

$$\bar{\omega} = \left(|\bar{S}| - \frac{g\beta}{Pr_t|\bar{S}|}\frac{\partial \bar{\theta}}{\partial x_j}\delta_{1j}\right). \tag{8}$$

For isothermal flows, both the Eidson model and the modified model return to the Smagorinsky model.

2.2. The SGS heat flux model

The linear isotropic eddy diffusivity model has been commonly used to model the SGS heat fluxes, h_j, stemming from the filtered thermal energy equation, (2), by taking the following form

$$h_j = \overline{u_j\theta} - \bar{u}_j\bar{\theta} = -\alpha_t\frac{\partial \bar{\theta}}{\partial x_j} = -\frac{\nu_t}{Pr_t}\frac{\partial \bar{\theta}}{\partial x_j}, \tag{9}$$

where α_t is the SGS diffusivity and

$$\alpha_t = C_t\bar{\Delta}^2\bar{\omega} = \frac{C}{Pr_t}\bar{\Delta}^2\bar{\omega}. \tag{10}$$

As mentioned above, the linear relation, Eq. (9), was assumed in deriving the Eidson model, Eq. (7), through the SGS production–dissipation equilibrium hypothesis. For a buoyant flow, the production term of the SGS kinetic energy consists of two parts: a strain-related production and a buoyancy production, i.e.

$$P_{k\mathrm{SGS}} = P_{k\mathrm{SGS}}^{\mathrm{s}} + P_{k\mathrm{SGS}}^{\mathrm{b}} = -\tau_{ij}\bar{S}_{ij} - \beta g_j h_j. \tag{11}$$

Provided that the dissipation is formulated in terms of $\bar{\Delta}$ and ν_t, we have

$$\varepsilon = C_\varepsilon\frac{\nu_t^3}{\bar{\Delta}^4}. \tag{12}$$

With the local equilibrium assumption for the SGS turbulence and using Eqs. (3), (11) and (12), a general formulation for the SGS eddy viscosity can be readily derived, which reads

$$\nu_t = C\bar{\Delta}^2\left(|\bar{S}|^2 - \frac{\beta}{\nu_t}g_i h_i\right)^{1/2}. \tag{13}$$

Since the effect of the subgrid scales is designated by the SGS model, it is possible that the modeling of the

SGS turbulence would to some extent modify the resolved turbulence with some properties similar to those of the modeled SGS turbulence. Such a conjecture is similar to the scale-similarity assumption, whose degree of confidence depends however on the filtering cutoff. It is reasonable from a time-averaging point of view to argue for a corresponding relation between the intensities of SGS turbulence and resolved large-scale turbulence. That is, undergoing a certain filtering, a resolved turbulence quantity with a large value would have a large SGS counterpart and vice versa. This argument may be applied to modeling the SGS stress/heat flux of which the magnitude should be in harmony with that of the corresponding resolved stress/heat-flux component.

The linear heat-flux model in Eq. (9) estimates the mean (time-averaged) SGS heat flux by means of the correlation of the SGS diffusivity and the large-scale temperature gradient. That is

$$\langle h_i \rangle = -\left\langle \alpha_t \frac{\partial \bar{\theta}}{\partial x_i} \right\rangle, \tag{14}$$

where the symbol $\langle\ \rangle$ denotes the time-averaging. For a fully developed channel flow with differentially heated walls where the mean temperature gradient vanishes in the streamwise (x_1) direction, it is known from experiments [8] that the resolved turbulent heat flux component in this direction is significantly larger than in the wall-normal direction (x_2). In this case, it is expected that the SGS heat fluxes comply with $|\langle h_1 \rangle| > |\langle h_2 \rangle|$. It is shown in the computation below that the linear model, as given by (14), will by contrast render a much lower correlation in the streamwise direction than in the wall normal direction.

It is noted here that the above modeling argument is based on a physically plausible hypothesis in analogy to the scale similarity which assumes scale-invariant turbulence properties for the subgrid scales and the smallest resolved scales. The present argument in other words suggests that the characteristic scales for the *mean* large-scale turbulence are in harmony with those for the *mean* SGS turbulence.

The basic motivation of this study is to replace the scalar SGS diffusivity with a tensorial one in the modeling of the SGS heat fluxes. An analogous idea has actually been suggested in the RANS modeling approach, for which Batchelor [9] suggested the use of a tensorial thermal diffusivity to model the heat flux vector, viz:

$$\langle u_i' \theta' \rangle = -D_{ik} \frac{\partial \langle \theta \rangle}{\partial x_k}, \tag{15}$$

where D_{ik} is the turbulent diffusivity tensor. The simplest model falling in line with (15) in RANS is the so-called *GGDH approach* [10], which expresses the turbulent heat flux vector as

$$\langle u_i' \theta' \rangle = -C_{\theta r} \tau \langle u_i' u_k' \rangle \frac{\partial \langle \theta \rangle}{\partial x_k}, \tag{16}$$

where $C_{\theta r}$ is a model constant and τ is an appropriate turbulent timescale.

While there have been a number of analyses of the turbulent heat flux in RANS modeling, see e.g. [8,11], very few have been reported on the behavior of the SGS heat-flux transport. It is unclear whether the same or a similar algebraic relation, which holds reasonably well in the RANS heat-flux transport, would hold as well for the SGS heat fluxes. Nevertheless, there have been some studies on non-linear modeling of the SGS stress, see e.g. [5,12]. For the SGS heat flux, however, little has been reported in terms of similar analyses. We directly invoke here an alignment assumption for the SGS heat flux in analogy to the RANS modeling approach.

It is well known that the generation of turbulent energy is essentially accomplished through large scales. The energy is then transferred in a cascade manner to the smaller and ever smaller scales and eventually dissipated by the smallest structure of Kolmogorov scales. In LES, we have the filtering cutoff in the inertial subrange of the energy spectra. The SGS scale itself would neither generate nor destroy but transfers (forward and backward) turbulent kinetic energy. Turning to the turbulence heat fluxes, we expect that analogous interchanges exist between the large and small scales. The transport equation for the SGS heat flux, h_i, can be symbolically written as

$$\frac{\partial h_i}{\partial t} + \frac{\partial}{\partial x_j}(\bar{u}_j h_i) = P_{i\theta} + G_{i\theta} + D_{i\theta} + D^{v}_{i\theta} + D^{p}_{i\theta} - \varepsilon^{v}_{i\theta}, \tag{17}$$

where the right-hand side includes subsequently the shear production, the buoyancy production, the SGS diffusion, the viscous diffusion, the pressure transport and the viscous dissipation [13]. The production terms in the transport equation take the following forms, respectively,

$$P_{i\theta} = -h_j \frac{\partial \bar{u}_i}{\partial x_j} - \tau_{ij} \frac{\partial \bar{\theta}}{\partial x_j}, \tag{18}$$

$$G_{i\theta} = -\beta g_i (\overline{\theta\theta} - \bar{\theta}\bar{\theta}). \tag{19}$$

Unlike in the RANS transport equation for turbulent heat fluxes, the production term for the SGS heat fluxes, $\Psi_{i\theta,\mathrm{SGS}} = (P_{i\theta} + G_{i\theta})$, represents actually the SGS heat flux *dissipation*. If $h_i > 0$, this SGS dissipation indicates the net heat flux exchange of forward ($\Psi_{i\theta,\mathrm{SGS}} > 0$) and backward ($\Psi_{i\theta,\mathrm{SGS}} < 0$) transfer between resolved large-scale and SGS thermal structures. If $h_i < 0$, forward (backward) transfer corresponds to $\Psi_{i\theta,\mathrm{SGS}} < 0$ ($\Psi_{i\theta,\mathrm{SGS}} > 0$).

It is thus reasonable to assume that the SGS heat flux is proportional to this net heat flux exchange. An

alignment between h_i and $\Psi_{i\theta,\mathrm{SGS}}$ can then be directly invoked as follows:

$$h_i = C_\theta \mathscr{T}_{\mathrm{SGS}}(P_{i\theta} + G_{i\theta}) = -C_\theta \mathscr{T}_{\mathrm{SGS}} \left(h_j \frac{\partial \bar{u}_i}{\partial x_j} + \tau_{ij} \frac{\partial \bar{\theta}}{\partial x_j} + \beta g_i k_\theta \right), \quad (20)$$

where C_θ is a scalar model coefficient, $\mathscr{T}_{\mathrm{SGS}}$ is an appropriate SGS timescale and $k_\theta = (\overline{\theta\theta} - \bar{\theta}\bar{\theta})$ is the SGS temperature variance. Since it is not intended to solve the k_θ equation, a model must be used for k_θ, which can be approximated by means of a local equilibrium assumption for the k_θ equation between its production, $-h_j(\partial\bar{\theta}/\partial x_j)$, and viscous dissipation, ε_θ, by approximating $\varepsilon_\theta \propto k_\theta/\mathscr{T}_{\mathrm{SGS}}$. This yields

$$k_\theta = -C_k \mathscr{T}_{\mathrm{SGS}} h_j \frac{\partial \bar{\theta}}{\partial x_j}, \quad (21)$$

where C_k is a scalar model coefficient.

Eqs. (20) and (21) form an implicit algebraic formulation for the SGS heat flux vector, h_i, which is rather complicated to solve in LES. The model invokes more than one model coefficient that need to be determined. Moreover, singularities can occur for certain types of behavior in the large-scale velocity and temperature gradients. Instead, Eq. (20) is further simplified here in terms of only the deviatoric part of the SGS stress tensor, τ^a_{ij}, and the large-scale temperature gradients. This renders

$$h_i = -C_\theta \mathscr{T}_{\mathrm{SGS}} \tau^a_{ij} \frac{\partial \bar{\theta}}{\partial x_j}, \quad (22)$$

where

$$\tau^a_{ij} = \tau_{ij} - \frac{\delta_{ij}}{3}\tau_{kk} = -2\nu_t S_{ij}.$$

Formulating the SGS timescale in terms of the filter size, $\bar{\Delta}$, and the SGS viscosity, ν_t, i.e. $\mathscr{T}_{\mathrm{SGS}} \propto \bar{\Delta}^2/\nu_t$, we get

$$h_i = C_t \bar{\Delta}^2 \bar{S}_{ik} \frac{\partial \bar{\theta}}{\partial x_k}, \quad (23)$$

where C_t is a model coefficient that can be determined using the dynamic procedure [14,15].

Unlike the isotropic diffusivity model, the proposed heat flux model invokes a tensor diffusivity and takes into account the temperature gradients in all directions for each heat flux component. The model is able to sustain the streamwise SGS heat flux through a cross-stream large-scale temperature gradient in the presence of SGS shear stress, even when the thermal gradient vanishes in the streamwise direction.

It is interesting to note that, in modeling the SGS stress, Leonard [6,16] applied the Taylor expansion to the filtering operation and reached a non-linear tensor eddy viscosity model from the Bardina scale-similarity model [17]. In the simplest form by a truncation of high-order terms, the Leonard expansion approximates the Bardina model as

$$\tau_{ij} = C_l \bar{\Delta}^2 \frac{\partial \bar{u}_i}{\partial x_k} \frac{\partial \bar{u}_j}{\partial x_k}, \quad (24)$$

where $C_l \sim \mathscr{O}(1)$ is a model constant.

Applying the Leonard expansion to the scale-similarity model for the SGS heat flux of Bardina type, one readily gets

$$h_i = C_{lh} \bar{\Delta}^2 \frac{\partial \bar{u}_i}{\partial x_k} \frac{\partial \bar{\theta}}{\partial x_k}, \quad (25)$$

where C_{lh} is a model constant. The proposed non-linear heat flux model, Eq. (23), is then found be similar to a scale-similarity model, as approximated in Eq. (25).

One of the main purposes of this work is to perform an a posterior examination of the tensor eddy-diffusivity model in comparison with the isotropic diffusivity model for modeling buoyant flows. In the computation, the SGS stress is represented by means of the linear eddy-viscosity formulation, Eq. (3), in which the SGS viscosity is computed using the Smagorinsky model, Eqs. (5) and (6). Eq. (13) may also be used to directly introduce the thermal effect of SGS into the ν_t formulation, in which the SGS heat flux vector is represented by Eq. (23), giving an implicit expression for ν_t. A further approximation may be used by invoking the SGS time scaling in Eq. (6), viz. $\mathscr{T}_{\mathrm{SGS}} \propto 1/|\bar{S}|$. The SGS viscosity can then be estimated from (13) as

$$\nu_t = C\bar{\Delta}^2 \left(|\bar{S}|^2 - \frac{\beta}{\sigma_t |\bar{S}|} g_i \bar{S}_{ik} \frac{\partial \bar{\theta}}{\partial x_k} \right)^{1/2}, \quad (26)$$

where $\sigma_t = (C/C_t)$. Note that σ_t in (26) is not the SGS Prandtl number, which must be specified (as a constant or iteratively calculated from C and C_t). In the simulation, we focus on the comparison of the tensor diffusivity model (hereafter *GGDH model*), Eq. (23), with the linear isotropic diffusivity model (hereafter *Linear model*), Eqs. (9) and (10), for the SGS heat fluxes. Both heat flux models have thus been used respectively in conjunction with the dynamic Smagorinsky model based on Eqs. (5) and (6), to account for the SGS stress by excluding the buoyancy-related term from the ν_t formulation.

The model coefficients in these models, C and C_t, are dynamically determined using the dynamic procedure [14]. The grid filter is denoted here by an overbar. The test filter, denoted by a curved overbar, has a width of $\hat{\bar{\Delta}} = 2\bar{\Delta}$, as proposed by Germano et al. [14] to extrapolate the information from the smallest resolved scales. The Germano identity reads

$$\mathscr{L}_{ij} = T_{ij} - \widehat{\tau_{ij}} = \widehat{\bar{u}_i}\widehat{\bar{u}_j} - \widehat{\bar{u}_i}\widehat{\bar{u}_j}. \quad (27)$$

For the heat fluxes, a similar identity holds as

$$\mathscr{E}_j = H_j - \widehat{h}_j = \widehat{\bar{u}_j\bar{\theta}} - \widehat{\bar{u}}_j\widehat{\bar{\theta}}. \tag{28}$$

The right-hand side residual stresses and fluxes in Eqs. (27) and (28) are resolvable quantities. Assuming a scale invariance for the filtered stress tensor and heat flux vector in scales on the test-filtering and grid-filtering levels, one can then formulate the test-grid scale stress tensor, T_{ij}, and heat flux vector, H_j, in analogy to their SGS counterparts. This suggests

$$\mathscr{L}_{ij} = -2C\widehat{\bar{\Delta}}^2\,\widehat{\bar{\omega}}\widehat{\bar{S}}_{ij} + 2C\bar{\Delta}^2\,\widehat{\bar{\omega}\bar{S}_{ij}} \tag{29}$$

and with GGDH model,

$$\mathscr{E}_j = C_t\widehat{\bar{\Delta}}^2\widehat{\bar{S}}_{jk}\frac{\widehat{\partial\bar{\theta}}}{\partial x_k} - C_t\bar{\Delta}^2\widehat{\bar{S}_{jk}\frac{\partial\bar{\theta}}{\partial x_k}}, \tag{30}$$

where C and C_t have been assumed to be independent of the test-filtering operation.

By means of the least squares approach [15], the model coefficient C is determined by

$$C = -\frac{\mathscr{L}_{ij}M_{ij}}{2M_{ij}M_{ij}} \tag{31}$$

with

$$M_{ij} = \widehat{\bar{\Delta}}^2\,\widehat{\bar{\omega}}\widehat{\bar{S}}_{ij} - \bar{\Delta}^2\,\widehat{\bar{\omega}\bar{S}_{ij}}. \tag{32}$$

Similarly, the coefficient C_t is determined by

$$C_t = \frac{\mathscr{E}_jQ_j}{Q_jQ_j}, \tag{33}$$

where

$$Q_j = \widehat{\bar{\Delta}}^2\,\widehat{\bar{S}}_{jk}\frac{\partial\widehat{\bar{\theta}}}{\partial x_k} - \bar{\Delta}^2\widehat{\bar{S}_{jk}\frac{\partial\bar{\theta}}{\partial x_k}}. \tag{34}$$

In the computation, to avoid numerical instability, the model coefficients have been assumed to be functions of time and of inhomogeneous directions. A spatial averaging for the numerators and denominators in (31) and (33) was thus done over the direction of flow homogeneity. The averaged model coefficients are then $C = C(t,x_i)$ and $C_t = C_t(t,x_i)$, with x_i as the direction of flow inhomogenity. In the computation below, the flow is inhomogeneous in the wall-normal (y or x_2) direction.

3. Numerical results

The proposed SGS heat flux model is examined in this section in LES for a buoyant flow in a vertical channel. Direct numerical simulations of this type of flow have been carried out by several research groups [18,19]. The flow is induced by two infinite, vertical, differentially heated walls. As a result of this configuration, the fully developed mean flow is essentially of a one-dimensional type in the vertical, streamwise (x) direction with no thermal stratification. Periodic boundary conditions are assumed in the streamwise and the spanwise (z) directions. The Rayleigh number, $Ra = g\beta\Delta\Theta h^3/\nu\alpha$, considered in the computation is 5.4×10^5, which is based on the gap width, $L_y = h$, and temperature difference, $\Delta\Theta = \Theta_h - \Theta_c$, between the two vertical isothermal walls (at $y = 0$ and $y = h$, respectively). The Prandtl number is $Pr = 0.71$. In the DNS by Boudjemadi et al. [18], a computational domain with the dimensions of $L_x\times L_y\times L_z = 2.5h\times h\times h$ was used in the x, y and z directions, respectively. This domain was used in the present simulation with a grid resolution of $66\times50\times34$ (hereafter termed D1). A larger computation domain, $L_x\times L_y\times L_z = 12h\times h\times 6h$, was employed by Versteegh and Nieuwstadt [19] in their DNS at the same Ra. The two groups of DNS give somewhat different results. For comparison, a larger computational domain was also employed in the present work. In this case, the extension of the domain is $L_x\times L_y\times L_z = 5h\times h\times 4h$, corresponding to a grid resolution of $98\times50\times50$ (hereafter termed D2). The grid was refined near the vertical walls with $y_1^+ = 0.88$, while uniform grid was used in the other two directions.

The differential governing equations were discretized using the finite volume method, and thereby the box filter is implicitly used. The second-order central differencing scheme was used for spatial discretization and the Crank–Nicolson scheme for temporal discretization. An implicit, fractional-step time-advancement method was used to solve the filtered governing equations. Boussinesq approximation was employed in the simulation, by which the fluid properties were evaluated on the basis of a reference temperature, $\Theta_r = (\Theta_h + \Theta_c)/2$. A symmetric Gauss–Seidel method was used to solve the discretized transport equations of momentum and temperature. The Poisson equation for the pressure is solved using the multigrid method. All the quantities were averaged over time and the homogeneous directions (xz-plane), denoted by $\langle\ \rangle$. The time step adopted in the computation is about $\Delta t = 0.0266h/U_b$, where the velocity scale $U_b = \sqrt{g\beta\Delta\Theta h}$. Typically, the time period used to obtain turbulence statistics is about 50,000Δt after the flow is fully developed.

The statistical results presented below have been normalized using U_b and $\Delta\Theta$. Fig. 1 shows the resolved mean streamwise velocity and mean temperature across the gap between the side walls. The two models show nearly identical predictions for the same domain. The results with different domains are rather different however. With the small domain (D1), both models obviously overpredict the mean velocity as compared with the DNS data of Boudjemadi et al. [18], for which the peak is overestimated by about 10%. The mean tem-

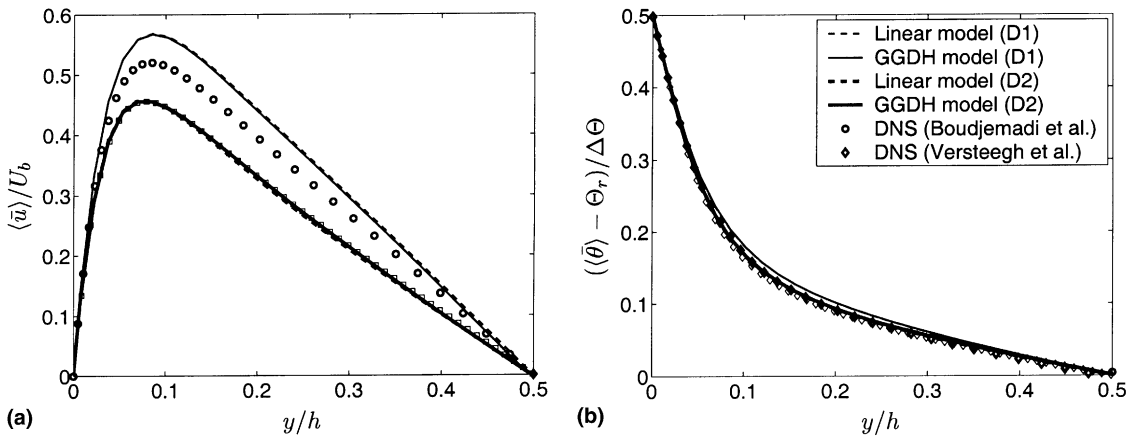

Fig. 1. Distribution of mean velocity and temperature: (a) mean streamwise velocity; (b) mean temperature.

perature is also slightly overpredicted by both models. Turning to the large domain (D2), the models nevertheless reproduce predictions that are in very good agreement with the DNS data of Versteegh and Nieuwstadt [19]. It should be noted that the numerical results depend on the domain size used for both LES and DNS. Since we have adopted periodic boundary conditions in the streamwise and spanwise directions, the computational domain in these directions should be at least twice as large as those of the largest turbulence scales, as pointed out by Versteegh and Nieuwstadt [19]. In the computation with the large domain (D2), the correlation functions were checked. It was found that the correlation reduces indeed to small values over a distance of half of the domain size at the present *Ra*.

The resolved velocity fluctuations are presented in Fig. 2. The streamwise velocity fluctuation, $\bar{u}_{\rm rms}$, is obviously overestimated by both models, Fig. 2(a), but with relatively larger discrepancies in the results of the linear model. This overprediction using the D1 domain is related in part to the overestimated mean velocity gradient, $\langle\partial\bar{u}/\partial y\rangle$, which, together with the resolved shear stress, $\langle u'v'\rangle$, contributes to the production of the streamwise resolved stress. On the other hand, buoyancy plays an important role through the streamwise resolved heat flux, although the mean temperature gradient vanishes in this direction. The buoyancy production for $\bar{u}_{\rm rms}$ actually dominates the shear production, as the velocity gradient changes sign near the wall [18]. As seen in Fig. 5(a), the resolved streamwise heat flux is indeed correspondingly overpredicted. The resolved wall-normal and spanwise velocity fluctuations, Fig. 2(b) and (c), rely on the resolved velocity–pressure–gradient correlation, which redistributes energy among the fluctuations. Both models have reproduced the two components reasonably well, giving nearly identical distributions for the same computational domain. The predicted wall-normal component, $\bar{v}_{\rm rms}$, is in nearly identical agreement with the DNS data for the D1 domain, Fig. 2(b), where, however, the spanwise fluctuation is overpredicted. For the D2 domain, $\bar{v}_{\rm rms}$ is underpredicted in comparison with the DNS data by Versteegh and Nieuwstadt [19], with which the spanwise components has reached good agreement.

Fig. 3 gives the distribution of the resolved temperature fluctuation. The results of both models are in very good agreement with DNS data using both computational domains. This implies that the production of $\bar{\theta}_{\rm rms}$ has been reasonably resolved in terms of the wall-normal heat flux, $\langle v'\theta'\rangle$, and the temperature gradient. This is indeed the case, as shown in Fig. 1 and as is identified in Fig. 5(b) for the distribution of $\langle v'\theta'\rangle$.

Fig. 4 shows the distribution of the resolved turbulent shear stress, $\langle u'v'\rangle$. The two models again yield very similar predictions that are in better agreement with the DNS data by Versteegh and Nieuwstadt [19] in the center of the channel. A budget analysis of the turbulent shear stress based on the DNS data [18] showed that most of the shear production takes place in the central part of the channel, while this production term becomes negative near the wall where the velocity gradient changes sign. The shear stress, however, remains positive owing to the large, positive buoyancy production in terms of the vertical streamwise heat flux $\langle u'\theta'\rangle$. Note that the streamwise heat flux would be predicted as zero when using a linear eddy-diffusivity model in RANS modeling and may consequently give a sign change in the shear stress, in contrast to the results given by DNS and by present LES.

Distribution of the resolved streamwise and wall-normal heat fluxes, $\langle u'\theta'\rangle$ and $\langle v'\theta'\rangle$ are shown in Fig. 5(a) and (b), respectively. With the D1 domain, both models reproduce $\langle u'\theta'\rangle$ an acceptable agreement with the DNS data, although they overestimate this quantity in the central region of the channel and the linear model underpredicts it in the outer part of the near wall

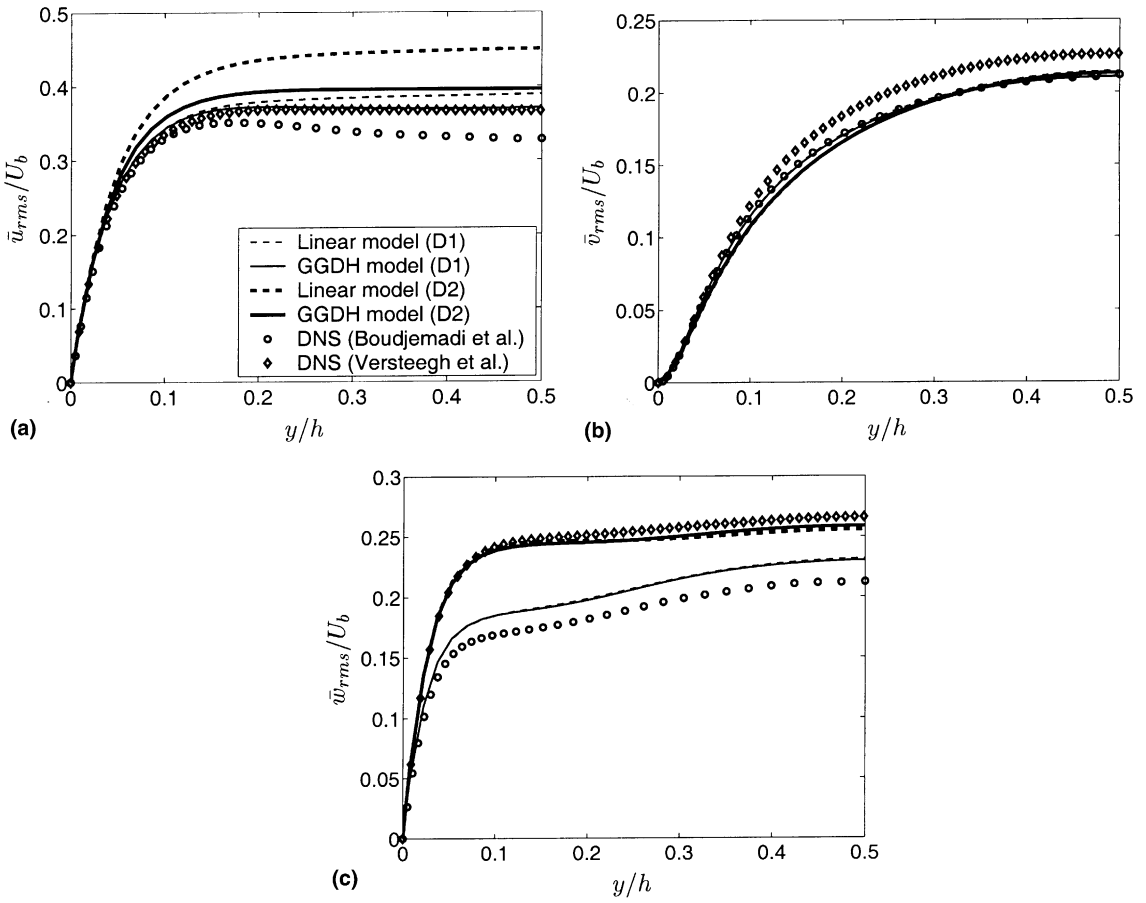

Fig. 2. Distributions of the resolved velocity fluctuations: (a) resolved streamwise velocity fluctuation; (b) resolved wall-normal velocity fluctuation; (c) resolved spanwise velocity fluctuation.

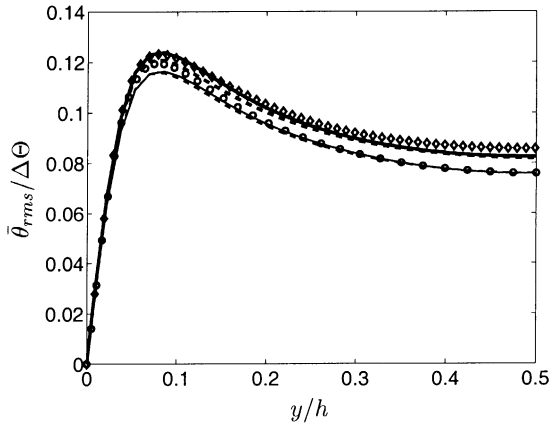

Fig. 3. Distribution of the resolved temperature fluctuation.

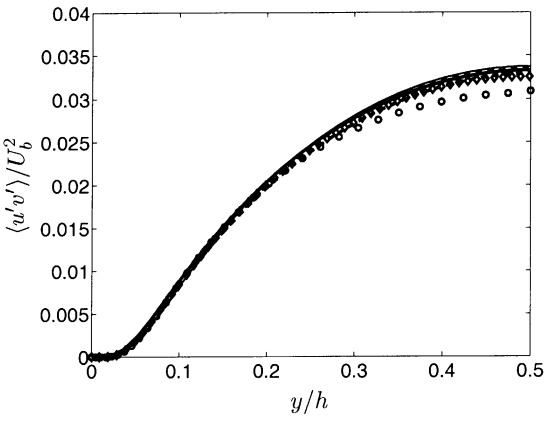

Fig. 4. Distributions for the resolved Reynolds shear stress.

boundary layer. With the D2 domain, large discrepancies arise for $\langle u'\theta'\rangle$ between the LES result and the DNS data. There may be several causes for this overprediction in $\langle u'\theta'\rangle$, including the overestimation of the resolved shear stress in the central part of the channel (Fig. 4) and the overestimated mean velocity gradient (with the D1

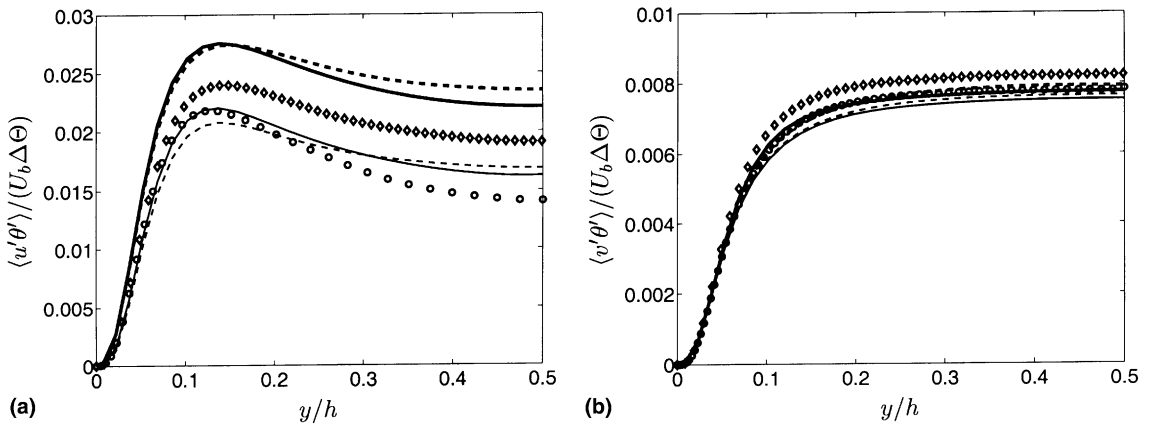

Fig. 5. Distributions of resolved turbulent heat fluxes: (a) resolved streamwise heat flux; (b) resolved wall-normal heat flux.

domain, see Fig. 1(a)). The two quantities contribute to the production of the resolved streamwise heat flux. Note that the grid resolution of D2 domain is coarser than that of the D1 domain (about 25% larger of the cell size in the streamwise direction). It is noted here that additional simulations were performed (not shown in this paper) with domains larger than the D2 domain, including the DNS domain by Versteegh and Nieuwstadt [19] and a domain with the dimensions of $L_x \times L_y \times L_z = 8h \times h \times 4h$, for which the same amount of grid nodes as in the D2 domain was used. It was found that the resolved streamwise heat flux is particularly sensitive to the grid resolution (or the computational domain). A coarse resolution (or a large computational domain) renders a large prediction in $\langle u'\theta'\rangle$, as is also shown in the two groups of DNS with different domains. Nevertheless, the resolved wall-normal heat flux is reproduced reasonably well as compared with the DNS data, Fig. 5(b). Note that the gradient production in the transport equation for $\langle v'\theta'\rangle$ is associated with the wall-normal stress component, $\langle v'v'\rangle$, which was reasonably reproduced by both models as shown in Fig. 2(b).

In general, the GGDH model yields predictions that are similar to those of the linear model, while the former is able to attain some visible improvements for the flow considered. Note that both models have been used in conjunction with the same SGS eddy viscosity model to handle the SGS stress. This implies that the modeling of the SGS heat flux gives its impact on the velocities essentially through the simulation of the large-scale thermal field, whereby the buoyancy impose its effects on the large-scale momentum transport in the streamwise (gravitational) direction and, consequently, modifies the large-scale turbulence structure and statistics. The effect of using different SGS heat flux models has indeed been reflected most sensitively in the streamwise velocity fluctuation, as shown in Fig. 2(a).

A straightforward means of observing to what degree the SGS effect has been represented is to look into the SGS statistics, which are directly approximated by the SGS model itself. The discussion below is based on the results obtained with the D2 domain. A comparison is made in Fig. 6 of the time-averaged model coefficients. The linear and GGDH heat flux models hardly exercise any difference in the model coefficient $\langle C\rangle$, Fig. 6(a), since it was dynamically determined using the same eddy viscosity model as the base model. As expected, nevertheless, the coefficient $\langle C_t\rangle$, Fig. 6(b), is very different for the two heat flux models. The coefficient of the GGDH model is about 4–5 times larger than that of the linear model. Both $\langle C\rangle$ and $\langle C_t\rangle$ remain approximately at a constant level in the central region of the channel. Fig. 6(c) illustrates the ratio $\sigma_t = \langle C\rangle/\langle C_t\rangle$. In a large part of the channel away from the wall, σ_t remains constant. For the GGDH mode, $\sigma_t \approx 0.075$ in the central part of the channel. For the linear model, σ_t is actually the SGS Prandtl number, Pr_t, which has remained at about 0.4 in the region away from the wall. This is the *standard* value of Pr_t recommended by Eidson [7], and is also recovered dynamically in LES for RB convection [1,3]. It seems that Pr_t is less dependent on flow problems than $\langle C\rangle$ and $\langle C_t\rangle$ and may be taken as a constant in simulations of a large range of thermal flows.

At the *Ra* number considered, the buoyant flow is characterized by a relatively low turbulence level. This may make the SGS turbulence less effective on large scales. Fig. 7 shows the distribution of time-averaged SGS eddy viscosity and its variance (normalized by the molecular one), $\langle \nu_t\rangle/\nu$, and $\nu_{t,\mathrm{rms}}/\nu$ with the GGDH model (the linear model gives nearly identical distributions). The time-averaged eddy viscosity is generally less than 30% of the molecular viscosity. It suggests that the simulated mean energy transfer from resolved to subgrid scales is rather weak. Moreover, although rather large instantaneous SGS viscosity (about 10 times larger than ν)

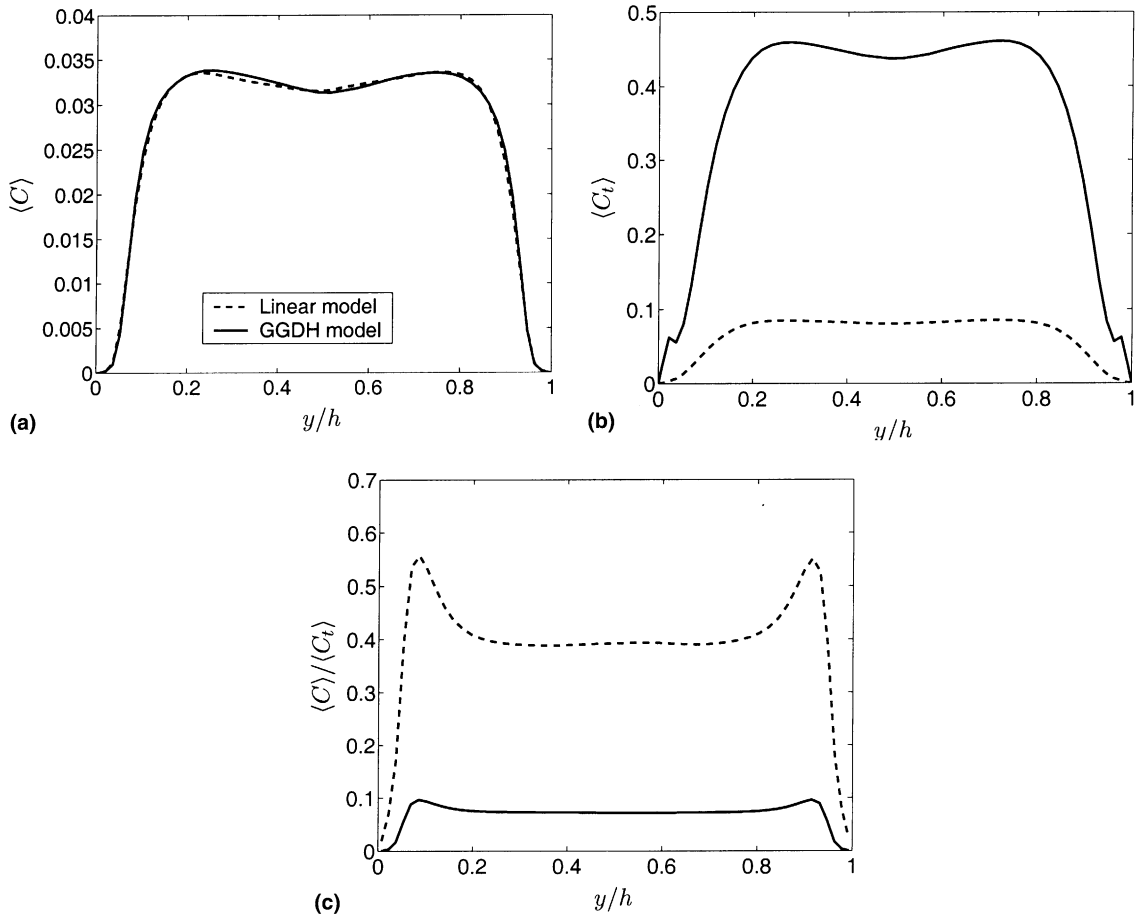

Fig. 6. Time-averaged model coefficients (D2 domain).

has been observed in the computation, the mean maximum energy transfer from large to small eddies represented by the SGS model in terms of $(\langle \nu_t \rangle + \nu_{t,\mathrm{rms}})$ is only marginally comparable with the viscous one, as illustrated in Fig. 7. To verify whether the present resolution is *over-refined*, a simulation was done with a coarse grid in the wall-normal direction (34 cells compared with the present 48 cells). It was found that the time-averaged SGS viscosity remains at about the same level as was obtained with the present grid. The weak energy occurrence between the large and subgrid scales may largely be due to the overall weak turbulence intensity in the flow considered. This will be discussed further below by means of an analysis of the energy spectra.

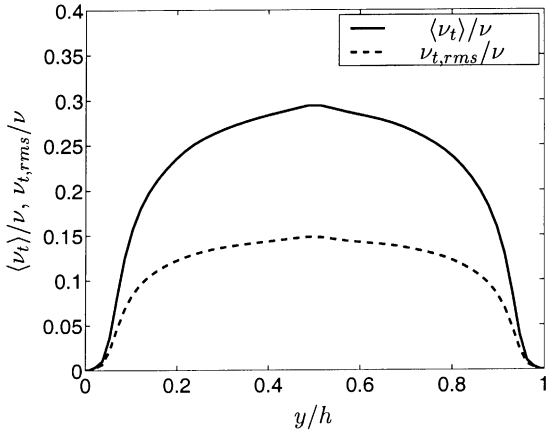

Fig. 7. Time-averaged SGS eddy viscosity and its fluctuation (GGDH model, D2 domain).

A more comprehensive illustration of the modeling of the effect of subgrid scales can be gained from the modeled SGS turbulence statistics. Fig. 8 plots the distributions of time-averaged SGS shear stress and heat fluxes. Again, the use of the same linear SGS stress model in conjunction with different heat flux models renders similar SGS shear stress, Fig. 8(a). Corresponding to the low SGS, viscosity, the time-averaged SGS shear stress, $\langle \tau_{12} \rangle$, is rather small in the channel center as compared with its resolved counterpart shown in Fig. 4. The linear and GGDH heat-flux models re-

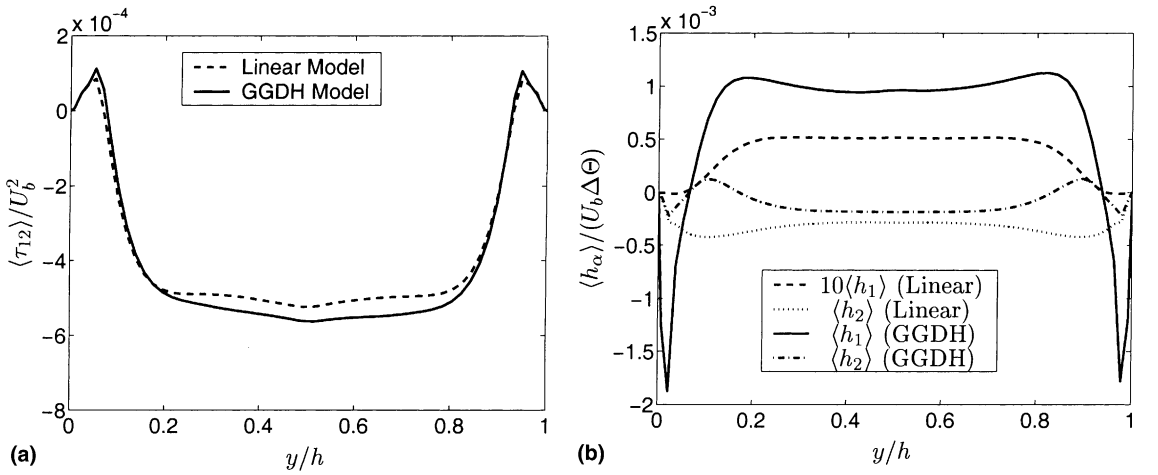

Fig. 8. Comparison of time-averaged SGS turbulence statistics (D2 domain): (a) SGS shear stress; (b) SGS heat fluxes, $\langle h_1 \rangle$ and $\langle h_2 \rangle$ in the streamwise and wall-normal direction, respectively.

produce various distributions of the SGS heat fluxes, as shown in Fig. 8(b). In the near-wall region, they are particularly comparable to the resolved heat fluxes presented in Fig. 5(a) and (b). Due to the statistically unstratified flow feature in the vertical streamwise direction, the linear model yields a negligibly small time-averaged SGS heat flux, $\langle h_1 \rangle$, as expressed by Eq. (14). Note that the linear model has generally yielded $|\langle h_1 \rangle| < |\langle h_2 \rangle|$. As we have argued, $|\langle h_1 \rangle|$ should be larger than $|\langle h_2 \rangle|$ in line with the fact that $\langle u'\theta' \rangle$ is larger that $\langle v'\theta' \rangle$. The GGDH model complies with this argument, as shown in Fig. 8(b), which gives indeed $|\langle h_1 \rangle| > |\langle h_2 \rangle|$, as desired.

It is interesting to note that the SGS turbulence statistics change sign at about the maximum velocity ($y/h \approx 0.085$ or $y^+ \approx 10.5$) in the near-wall boundary layer, as shown in Fig. 8(b), while this is not the case for $\langle h_2 \rangle$ with the linear model, which nevertheless keeps overall negative values owing to the positive temperature gradient across the channel. The small value of $\langle h_1 \rangle$ produced by the linear model implies a weak correction between the SGS diffusivity and the large-scale temperature gradient in the streamwise direction. Because of the relatively strong correlation between the large-scale strain rate and the temperature gradient, $\langle \bar{S}_{12}(\partial\bar{\theta}/\partial x_2) \rangle$, the GGDH model by contrast has significantly enhanced $\langle h_1 \rangle$. The result is opposite for the wall-normal SGS heat-flux component, $\langle h_2 \rangle$, for which the GGDH model yields smaller values than does the linear model, because the large strain rate and the cross-stream temperature gradient, $\bar{S}_{21}$ and $(\partial\bar{\theta}/\partial x_2)$, are respectively diminished by small values of $(\partial\bar{\theta}/\partial x_1)$ and $\bar{S}_{22}$.

As pointed out previously, the GGDH heat flux model is somewhat similar to a scale-similarity model of Bardina type. In a priori tests [17], the scale-similarity model for SGS stresses was verified to account for an excessive amount of energy backscatter. In an analysis of the production term (representing the SGS heat-flux dissipation) in the transport equation of SGS heat-flux, it was found that the GGDH model has yielded a large amount of backward (reverse) transfer particularly for the wall-normal heat flux as compared with the linear model [13].

It is known that a well-resolved LES should have the filtering cutoff in the inertial subrange of the energy spectrum, where the energy decays with wave number, k as $k^{-5/3}$. For turbulent thermal flows with appreciable buoyant influence, a number of experimental measurements have shown that a so-called *buoyancy subrange* with steep dependence on k exists next to the $k^{-5/3}$ subrange in the energy spectra [20–22]. The buoyancy subrange is characterized by k^{-m} dependence with $m > 5/3$, as asserted by Lumley [23]. In Fig. 9, we plot the one-dimensional spectra for the filtered velocity and temperature as functions of wave numbers in the streamwise direction, k_x. They are computed from the GGDH model based on the D2 domain (the spectra by the linear model are very similar). The resolution barrier in the streamwise (x) direction is $k_{xc} = \pi/\Delta_x \approx 603$. The spectra are obtained at two different points, $y^+ \approx 17$ and 60, respectively, located outside of the velocity peak and near the channel center. It is shown that the inertial subrange with $k^{-5/3}$ is not as extended owing to the relatively low *Ra* number considered. For both the velocity and thermal fluctuations, the spectra indeed exhibit a k^{-3} buoyancy subrange at large wave numbers, where the turbulence is rather isotropic. The buoyancy force has appreciably modified the transformation of the potential energy to kinetic energy with an efficiency that decreases with increasing the eddy size (with small wave

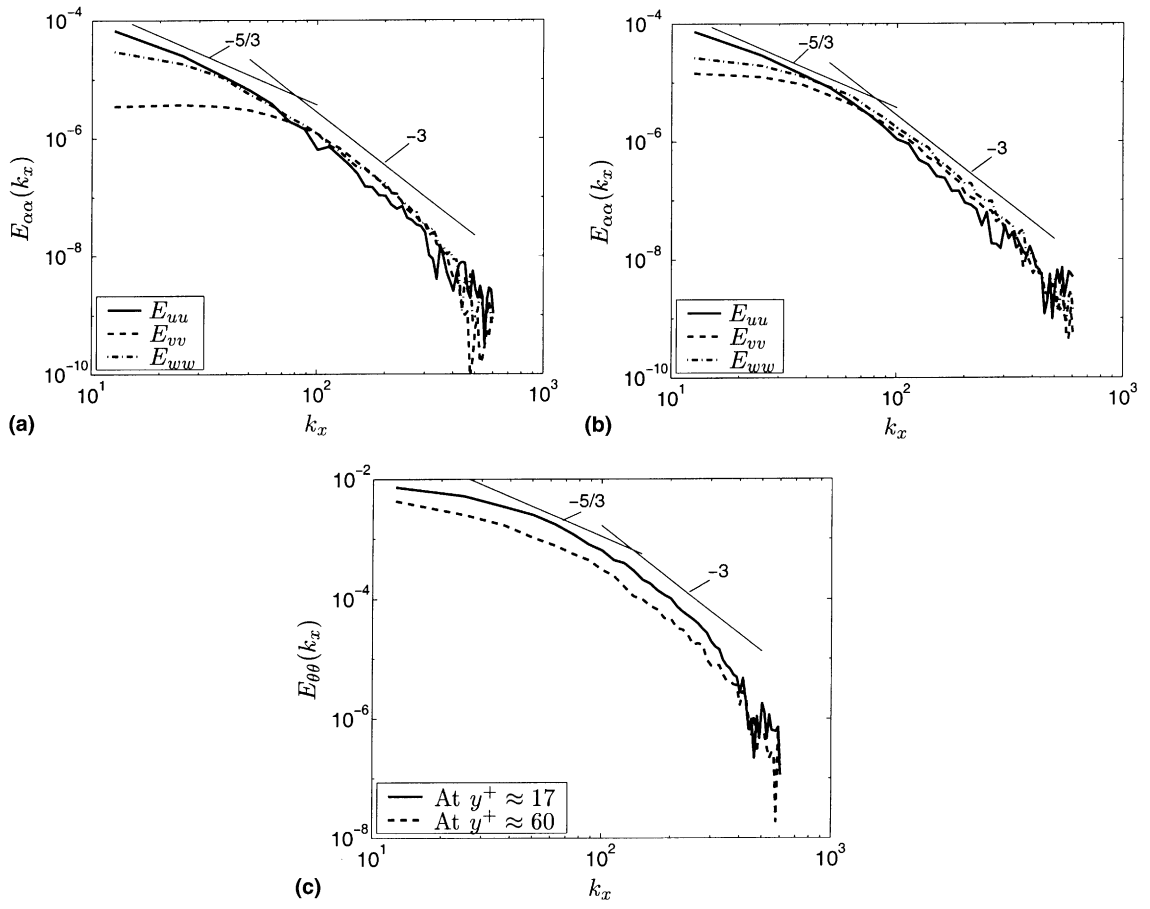

Fig. 9. One-dimensional spectra vs wavenumbers in the streamwise direction: (a) spectra for velocity fluctuations at $y^+ \approx 17$ ($y/h = 0.1383$); (b) spectra for velocity fluctuations at $y^+ \approx 60$ ($y/h = 0.4857$); (c) spectra for temperature fluctuations at two locations.

numbers). In the central part ($y^+ \approx 60$ in Fig. 9(b)), the flow is more isotropic than at the location in the boundary layer ($y^+ \approx 17$ in Fig. 9(a)), where the thermal fluctuation is relatively intensive (Fig. 9(c)).

4. Conclusions

A non-linear SGS heat-flux model was proposed in large eddy simulations of turbulent thermal flows. The physical reasoning for formulating the present model was discussed. The model was examined in large eddy simulation for the buoyant flow in a vertical channel with differentially heated side walls. The model is able to yield very encouraging results as compared with the isotropic SGS diffusivity model and DNS data.

The proposal SGS heat-flux model does not employ a scalar SGS diffusivity. It is similar to some extent to the GGDH approach in statistical RANS modeling, yet is more plausible for subgrid turbulence by assuming that the SGS heat flux is proportional to the SGS heat-flux dissipation between the resolved and subgrid scales. It is argued that the mean SGS turbulence statistics represented by the SGS model should be in harmony with its mean resolved counterpart in the reduction or increment of turbulence intensity. Corresponding to the resolved turbulent heat fluxes, of which the streamwise component is, for example, larger than the wall-normal one as in an infinite cavity flow where the statistical thermal gradient vanishes in the streamwise direction, the GGDH model renders a mean streamwise SGS heat flux larger than that in the wall-normal direction. In estimation of the SGS thermal turbulence, the GGDH SGS heat flux model is shown to be generally different from the isotropic SGS diffusivity model.

The proposed model formulates the SGS heat flux in terms of the large-scale strain rate and the temperature gradient in all directions. In the presence of SGS stresses, it thus enables the large-scale thermal gradient in other directions to modify the SGS heat flux in the

direction with no statistical temperature gradient. The model turns out to be similar to a scale-similarity heat flux model, provided that the Leonard expansion is applied to a scale-similarity heat flux model of the Bardina type.

Finally, it is noted here that the main purpose of this work is to present the non-linear (GGDH) SGS heat flux model and to examine its performance in large eddy simulation for turbulent thermal flows in comparison with the linear isotropic SGS diffusivity model. Admittedly, the Ra in the present test case is relatively low, which has somewhat made the SGS model less effective in the simulation. To proceed with comprehensive analyses of the model in representing the flow physics, it is preferable to perform a priori tests with DNS data. To gain more perceptive insight of the model, on the other hand, extensive a posterior simulations must be carried out for flows with intensive turbulence and significant heat transfer.

Acknowledgements

This work was supported in part by TFR (the Swedish Research Council for Engineering Sciences). Computer time on the SGI ORIGIN 2000 machines at UNICC, Chalmers, is gratefully acknowledged.

References

[1] W. Cabot, Large-eddy simulations of time-dependent and buoyancy-driven channel flows, in: Annual Research Briefs, Center for Turbulent Research, Stanford University/NASA Ames Research Center, 1992, pp. 45–60.
[2] V.M. Canuto, M.S. Dubovikov, A. Dienstfrey, A dynamic model for turbulence: IV. Buoyancy-driven flows, Phys. Fluids A 9 (1997) 2118–2131.
[3] S.-H. Peng, L. Davidson, Comparison of subgrid-scale models in LES for turbulent convection flow with heat transfer, in: Turbulent Heat Transfer, Manchester, UK, vol. 2, 1998, pp. 5.24–5.35.
[4] T.S. Lund, E.A. Novikov, Parameterization of subgrid-scale stress by the velocity gradient tensor, in: Annual Research Briefs, Center for Turbulent Research, Stanford University/NASA Ames Research Center, 1992, pp. 27–43.
[5] B. Kosovic, Subgrid-scale modelling for the large-eddy simulation of high-Reynolds-number boundary layer, J. Fluid Mech. 336 (1997) 151–182.
[6] A. Leonard, Energy cascade in large-eddy simulations of turbulent fluids flows, Adv. Geophys. 18A (1974) 248–273.
[7] T.M. Eidson, Numerical simulation of the turbulent Rayleigh–Bénard problem using subgrid modelling, J. Fluid Mech. 158 (1985) 245–268.
[8] B.E. Launder, On the computation of convective heat transfer in complex turbulent flows, ASME J. Heat Transfer 110 (1988) 1112–1128.
[9] G.K. Batchelor, Diffusion in a field of homogeneous turbulence, Aust. J. Sci. Res. (1949) 437–450.
[10] B.J. Daly, F.H. Harlow, Transport equations in turbulence, Phys. Fluids 13 (1970) 2634–2649.
[11] H. Kawamura, Y. Kurihara, Modelling of turbulent scalar transport in homogeneous turbulence, Int. J. Heat Mass Transfer 43 (2000) 1935–1945.
[12] V. Borue, S.A. Orszag, Local energy flux and subgrid-scale in three-dimensional turbulence, J. Fluid Mech. 366 (1998) 1–31.
[13] S.-H. Peng, L. Davidson, A proposed nonlinear SGS heat flux model for large eddy simulation of turbulent buoyant flow. Technical Report 01/03, Department of Thermo and Fluid Dynamics, Chalmers University of Technology, Gothenborg, 2001.
[14] M. Germano, U. Piomelli, P. Moin, W.H. Cabot, A dynamic subgrid-scale eddy viscosity model, Phys. Fluid A 3 (1991) 1760–1765.
[15] D.K. Lilly, A proposed modification of the Germano subgrid-scale closure method, Phys. Fluids A 4 (1992) 633–635.
[16] A. Leonard, Large-eddy simulation of chaotic convection and beyond, AIAA Paper 97-0204, Reno, 1997.
[17] J. Bardina, J.H. Ferziger, and W.C. Reynolds, Improved subgrid scale models for large eddy simulation, AIAA Paper 80–1357, Snomass, Colorado, 1980.
[18] R. Boudjemadi, V. Manupu, D. Laurence, P. Le Quere, Budgets of turbulent stresses and fluxes in a vertical slot natural convection flow at Rayleigh $Ra = 10^5$ and 5.4×10^5, Int. J. Heat Fluid Flow 18 (1997) 70–79.
[19] T.A.M. Versteegh, F.T.M. Nieuwstadt, Coherent structure in natural convection between two vertical, differentially heated walls, in: Proceedings of the 2nd International Symposium on Turbulence, Heat and Mass Transfer, Delft, 1997.
[20] D.D. Papailiou, P.S. Lykoudis, Turbulent free convection flow, Int. J. Heat Mass Transfer 17 (1974) 161–172.
[21] R.G. Bill, B. Gebhart, The development of turbulent transport in a vertical natural convection boundary layer, Int. J. Heat Mass Transfer 22 (1979) 267–277.
[22] N.E. Kotsovinos, Turbulence spectra in free convection flow, Phys. Fluids A 3 (1) (1991) 163–167.
[23] J.L. Lumley, The spectrum of nearly inertial turbulence in a stably stratified fluid, J. Atmos. Sci. 21 (1964) 99–121.